The Measurement of Water Salinity for Antarctic Research

Presented by:
Zuhayr Loonat

Prepared for:
Justin Pead
Dept. of Electrical Engineering
University of Cape Town

Submitted to the Department of Electrical Engineering at the University of Cape Town in partial fulfilment of the academic requirements for a Bachelor of Science degree in Electrical and Computer Engineering

October 26, 2025

Declaration

1. I know that plagiarism is wrong. Plagiarism is to use another's work and pretend that it is one's own.

2. I have used the IEEE convention for citation and referencing. Each contribution to, and quotation in, this report 'The Measurement of Water Salinity for Antarctic Research' from the work(s) of other people has been attributed and has been cited and referenced. Any section taken from an internet source has been referenced to that source.

3. This report 'The Measurement of Water Salinity for Antarctic Research' is my own work and is in my own words (except where I have attributed it to others).

4. I have not paid a third party to complete my work on my behalf. My use of artificial intelligence software has been limited to giving overviews of topics, checking grammar, aiding with LaTeX commands, and aiding with making BibTeX citations of sources (specify precisely how you used AI to assist with this assignment, and then give examples of the prompts you used in your first appendix).

5. I have not allowed and will not allow anyone to copy my work with the intention of passing it off as his or her own work.

6. I acknowledge that copying someone else's assignment or essay, or part of it, is wrong, and declare that this is my own work

Signature:..........................   Date: October 26, 2025

Zuhayr Loonat

Word Count:

Acknowledgments

I would like to express my sincere gratitude to my supervisor, Justin Pead, for his invaluable guidance, support, and expertise throughout this research. His insights and encouragement were instrumental in bringing this work to fruition.

I am also deeply grateful to my friends for their unwavering moral support during this journey. Their encouragement and understanding made the challenges of this process far more manageable.

Lastly, I would like to thank my family for their support during my studies.

Abstract

Ice shelves form when glaciers flow from the Antarctic out over the ocean. This ice, which is originally freshwater ice is formed from accumulated snow, extends over the water and floats, because ice is less dense than water. When saltwater freezes at the bottom of the ice shelves, salt is expelled, forming a brine like solution, with a high salt density, directly under the ice shelves.

The salinity of this brine solution and the seawater underneath need to be measured to aid in Antarctic research. This project documents the design and testing of a conductivity-based salinity measuring device to measure the salt content in these areas. The prototype was designed in two parts, a probe module, which would be lowered down through a water tower, which was drilled into the ice shelves, to measure the salinity, and a controller, which would be used to send instructions and receive data from the probe. The probe utilised gold electrodes to measure and analyse the salinity through conductivity. Two methods were investigated, Direct Current (DC), where point voltage measurements and voltage sweeps were conducted, and Alternating Current (AC) where a machine learning model was used to map properties of the input and output waves to a salinity value. [Talk about accuracy TODO]

Contents

Glossary

AC Alternating Current iii, 21, 24, 29, 30

ADC Analogue to Digital Converter 21, 23, 24, 28, 29, 30, 34, 35

ANN Artificial Neural Network 15

CTD Conductivity, Temperature, Depth 12, 17, 18

DAC Digital to Analogue Converter 21, 24, 26, 28, 29, 30, 32, 34, 35

DC Direct Current iii, 21, 29, 30, 34

EEC Equivalent Electrical Circuit 14

EIS Electrochemical Impedance Spectroscopy v, 5, 13, 14, 30, 31, 32

ENIG Electroless Nickel Immersion Gold 18

IC Integrated Circuit 21, 24, 25, 26, 27

LED Light Emitting Diode 25, 26

ML Machine Learning 5, 33

PCB Printed Circuit Board 18, 19, 20, 21, 24, 25, 27, 33

PSU Practical Salinity Unit 6, 10, 12, 30, 38, 41

UART Universal Asynchronous Receiver-Transmitter 24

‰ Parts per thousand 6, 8

Chapter 1

Introduction

1.1 Background to the study

A very brief background to your area of research. Start off with a general introduction to the area and then narrow it down to your focus area. Used to set the scene[**?**].

1.2 Objectives of this study

1.2.1 Problems to be investigated

Description of the main questions to be investigated in this study.

1.2.2 Purpose of the study

Give the significance of investigating these problems. It must be obvious why you are doing this study and why it is relevant.

1.3   Scope and Limitations

Scope indicates to the reader what has and has not been included in the study. Limitations tell the reader what factors influenced the study such as sample size, time etc. It is not a section for excuses as to why your project may or may not have worked.

1.4   Plan of development

Here you tell the reader how your report has been organised and what is included in each chapter.

I recommend that you write this section last. You can then tailor it to your report.

Chapter 2

Literature Review

2.1 Introduction

Accurate salinity measurement is fundamental to oceanographic research. Traditional measurement techniques have evolved from labour-intensive chemical titration methods to modern electronic sensors, with electrical conductivity emerging as the predominant approach due to its combination of accuracy, speed, and practical deployability. This literature review examines the current state of salinity measurement technology with particular emphasis on conductivity-based methods and emerging machine learning approaches for electrochemical data interpretation. The review is organised into three main sections. First, we establish the fundamental concepts of salinity and provide a comprehensive comparison of available measurement techniques. Second, we examine the theoretical foundations and practical implementation of electrical conductivity measurements for salinity determination, including instrumentation, calibration procedures, and current limitations. Finally, we explore the application of EIS and Machine Learning (ML) as advanced approaches for enhanced salinity analysis, examining how frequency-domain measurements and intelligent data processing can overcome limitations of traditional single-frequency conductivity methods. This comprehensive review provides the theoretical and methodological foundation for developing a machine learning-enhanced impedance spectroscopy approach for salinity determination.

2.2 Salinity: Definition

Salinity is a fundamental characteristic of water, and is most commonly defined as the total amount of dissolved salts in water, and in the context of oceanography, seawater. It is typically expressed in Parts per thousand (‰) or Practical Salinity Unit (PSU) [1]. The concept of salinity has evolved significantly from its early definition, which was based on chlorinity measurements. Modern salinty is defined through the Practical Salinity Scale 1978 (PSS-78), where salinity is based on the conductivity ratio of standard seawater solutions, to a standard Potassium Chloride solution, and is dimensionless [2]. The salinity-conductivity relationship is however, quite complex, requiring corrections and calibrations needed for depth and temperature, as these both play a factor in the conductivity of the water.

2.3 Overview of Salinity Measurement Methods

There are a multitude of methods which can be used to measure salinity, each with their own advatages, limitations and levels of accuracy. Traditional methods include gravimetric analysis, chemical titration (such as the Mohr-Knudsen method for chlorinity), and refractometry. While these techniques can provide accurate results, they are often time-consuming, require skilled operators, and are not easily adaptable to in-situ or automated measurements. Modern approaches predominantly rely on electrical conductivity sensors, which offer rapid, repeatable, and automated salinity determination. Other techniques, such as optical methods and ion-selective electrodes, have also been explored, but are less commonly used in oceanographic applications due to issues with robustness, calibration, or specificity. The choice of method depends on the required accuracy, operational environment, and available resources.

2.3.1 Historical Methods

Chlorinity Titration

Early salinity measurements relied on chemical titration methods, in particular the Mohr-Knudsen chlorinity titration, which used silver nitrate. The chlorinity of a solution has the definition 'the mass of silver required to precipitate completely the halogens in

0.3285234kg of sample seawater'. This method was highly accurate, with results within ($\pm$0.001 PSU). However, it relied heavily on toxic chemicals, and was a time-consuming laboratory procedure, with limited practical application in the field [3].

Gravimetric Methods

Gravimetric analysis, a technique used to determine an amount of a substance, by measuring its change in mass, invloves evaporation and the weighing of dissovled solids. This method directly provided measurements of the salt content, within accuracies of ($\pm$0.001 PSU), under controlled laboratory conditions. This method remains the reference standard for calibration processes, but is however, extremely slow [4].

2.3.2   Physical Property Based Methods

There are several methods that utilise the relationship between salinity and the physical properties of water.

Hydrometric and Density Methods

Hydrometric methods using density measurements via hydrometers, offer salinity measurements that are low-cost, and electronics free. However, they are limited in precision with accuracies of $\pm 1 - 2$ PSU, and require large sample volumes. The hydrometer is a floating instrument, that sinks to different depths depending on the density of the solution, and by measuring how high or low it floats, the density of the solution can be determined [5]. The following equation is used to map the relationship between salinity and density [6].

$$\rho = \rho_0(1 + kS) \tag{2.1}$$

where ρ is the density, ρ_0 is the density of fresh water, S is the salinity and k is the proportionality constant.

This can then be inverted to give Salinity from Density:

$$S = \frac{\frac{\rho}{\rho_0} - 1}{k} \tag{2.2}$$

This however, does not include temperature correction.

Refractometric Thechniques

Refractometric techniques measure the refractive index changes cuased by the dissovled salts. The refractive index of seawater is influenced by wavelength, temperature, salinity, and pressure. Within the range of 500-700 nm wavelength, 0-30°C temperature, 0-40 PSU salinity, and 0-11000 dbar pressure, the refractive index equation provides an accuracy of 0.4-80 ppm PSU, with accuracy decreasing as pressure increases [7]. Refractometers, which require only a small sample volume, are compact devices, making them suitable for portable field measurements [8]. Fibre optic refractometers have improved portability and reduced temperature sensitivity, with moderate accuracy ($\pm$0.5-1 PSU), making them increasingly popular in aquaculture applications [9].

Freezing Point Osmometry

Freezing point depression osmometry exploits the colligative (i.e. relating to the binding together of molecules) properties of dissolved salts. The main principle relies on freezing point depression, which is the phenomenon where a solvents freeving point is lowered when a solute is added to it. To perform the measurement, the water is cooled till its freezing point and the temperature drop is measured, which is then used to calculate the osmolality [10]. This method can achieve accuracies of $\pm 2 mOsm/kgH_2O$ which is approximately $\pm 0.1 - 0.2$ ‰. However its requirement for precise temperature control limits its usage to laboratory applications [11].

Magnetic Permeability

Magnetic properties of liquids, particularly magnetic susceptibility, vary with ion concentration, offering a potential method for salinity determination. Research has demonstrated that bulk magnetic susceptibility (BMS) of saline water correlates with salinity and conductivity measurements, with water quality parameters exhibiting an inverse relationship with magnetic susceptibility values. This approach offers the benefit of non-contact measurement,

potentially avoiding sample contamination or disturbance [12]. However, the technique requires sophisticated instrumentation, which are typically designed for laboratory use rather than field deployment.

2.3.3 Advanced Analytical Methods

Ion Chromatography

Ion chromatography is an analytical technique used to separate and quantify ionic species in solution, making it highly valuable for determining the individual ion concentrations in seawater samples [13]. The method works by passing a liquid sample through a column containing special resin beads that selectively hold onto different ions. As a liquid solution flows through, ions are released at different times based on their properties and detected by measuring electrical conductivity. For seawater analysis, ion chromatography can separately measure major ions like chloride, sulfate, sodium, magnesium, calcium, and potassium, providing detailed compositional data rather than just total salinity. The technique offers high precision and can detect ions at very low concentrations, though it requires more sophisticated equipment and longer analysis times compared to simpler methods [14].

2.4 Conductivity-Based Salinity Measurements

2.4.1 Theoretical Foundation

Electrical conductivity has emerged as the predominant method for salinity measurement due to its practical implementation, high accuracy and fast response time. The technique utilises the strong correlation between dissolved ionic content and electrical conductivity.

The conductivity of a liquid is measured by its ability to conduct electrical current. The relationship between conductivity and salinity is based on the concentration of dissolved ions in seawater. The main ions found in sea water ($Na^+, Cl^-, Mg^{2+}, SO_4^{2-}, Ca^{2+}, K^+$) maintain a relatively constant proportional relationship, in ocean waters [4]. This enables robust corrections between conductivity and total dissolved salt content. Unlike other measurement techniques, conductivity accounts for all the ions in the water, not only

chlorine, which is why it is considered a more accurate measure of salinity [15].

The Practical Salinity Scale 1978 (PSS-78) defines Practical Salinity S_p through the conductivity ratio K_{15}, as shown below [16]:

$$K_{15} = \frac{C(S_p, 15, 0)}{C(KCl, 15, 0)} \tag{2.3}$$

where the numerator, $C(S, 15, 0)$ represents the conductivity of seawater sample at 15°C and standard atmospheric pressure ($1atm/101.325kPa/0dbar$), and the denomimator, $C(KCl, 15, 0)$ is the conductivity of a standard KCl (Potassium Chloride) solution under identical temperature and pressure. The standard KCl solution consists of $32.4356 \times 10^{-3}kg$ of KCl dissolved in $1kg$ of water [3]. When the ratio between the water sample and the KCl solution is 1, i.e. $K_{15} = 1$, then the Practical Salinity S_p is, according to the definition, 35 [16].

It is important to note that Practical Salinity is a unit-less quantity, and though it may be convenient, it would be incorrect to quote it in PSU. Practical salinity should rather be quoted as a certain Practical Salinity 'on the Practical Salinity Scale PSS-78' [16].

When K_{15} does not equal 1, Practical Salinity, S_p can be calculated using the equation below [16]:

$$S_p = \sum_{i=0}^{5} a_i (K_{15})^{i/2} \tag{2.4}$$

where K_{15} is the equation defined above (Equation 2.3), and the coefficients a_i are given in Table (2.1).

2.4.2 Temperature and Pressure Compensation

When calculating salinity at conditions other than 15°C, and $0dbar$, the conductivity ratio R is expanded to the product of three ratios R_p, R_t and r_t as follows [16]:

$$R = \frac{C(S_p, t, p)}{C(35, 15, 0)} = R_p R_t r_t \tag{2.5}$$

where t, and p are the temperature and pressure valid over the ranges $-2°C \leq t \leq 35°C$

and $0 \leq p \leq 10000 dbar$ respectively.

These ratios can be expanded as follows:

$$R = \frac{C(S_p, t, p)}{C(35, 15°C, 0)} = \frac{C(S_p, t, p)}{C(S_p, t, 0)} \cdot \frac{C(S_p, t, 0)}{C(35, t, 0)} \cdot \frac{C(35, t, 0)}{C(35, 15°C, 0)} = R_p R_t r_t \tag{2.6}$$

This equation represents the ratio between the conductivity measurement of a sample $C(S_p, t, p)$ and the conductivity of the standard solution $C(35, 15°, 0)$ [16]. In order to find the salinity, R_p, R_t and r_t need to be caculated. First, r_t is calculated using the temperature of the sample:

$$r_t = \sum_{i=0}^{4} c_i t_i \tag{2.7}$$

R_p is then calculated as a function of the temperature t, pressure p, and conductivity ratio R:

$$R_p = 1 + \frac{\sum_{i=1}^{3} e_i p^i}{1 + d_1 t + d_2 t^2 + R[d_3 + d_4 t]} \tag{2.8}$$

Finally, R_t can be evaluated using R, R_p and r_t:

$$R_t = \frac{R}{R_p r_t} \tag{2.9}$$

At standard conditions, i.e., temperature $t = 15°C$, R_t is equal to K_{15} an therefore Practical salinity S_p can be calculated from Equation 2.3. For cases where the temperature is not $t = 15°C$, Practical Salinity S_p is given as a function of R_t, with $k = 0.0162$ [16]:

$$S_p = \sum_{i=0}^{5} a_i (R_t)^{i/2} + \frac{t - 15}{1 + k(t - 15)} \sum_{i=0}^{5} b_i (R_t)^{i/2} \tag{2.10}$$

Note that Equations (2.3) to (2.10) are only valid in the range $2 < S_p < 42$, $-2°C \leq t \leq 35°C$ and $0 \leq p \leq 10000 dbar$.

It must be noted that the PSS-78 equations use the IPTS-68 temperature scale and in order for them to work with the current ITS-90 scale, must be converted using the equation below [16]:

$$t_{68}°C = 1.00024 \times t_{90}°C \tag{2.11}$$

i	a_i	b_i	c_i	d_i	e_i
0	0.0080	0.0005	$6.766\,097 \times 10^{-1}$		
1	−0.1692	−0.0056	$2.005\,64 \times 10^{-2}$	3.426×10^{-2}	2.070×10^{-5}
2	25.3851	−0.0066	$1.104\,259 \times 10^{-4}$	4.464×10^{-4}	-6.370×10^{-10}
3	14.0941	−0.0375	-6.9698×10^{-7}	4.215×10^{-1}	3.989×10^{-15}
4	−7.0261	0.0636	1.0031×10^{-9}	-3.107×10^{-3}	
5	2.7081	−0.0144			

Table 2.1: Table of Coefficients for PSS-78 Equations [16]

2.4.3   Instrumentation and Technology

The most common method for measuring salinity is by using a Conductivity, Temperature, Depth (CTD) device. The fundamental concept behind these devices involves placing two electrodes in a sample of water, applying a voltage across them and measuring the water's response. This is then paired with a temperature and depth correction, allowing for an accurate salinity measurement. The depth value for these calculations is taken from the pressure at which the measurement is taken. This pressure is then translated to depth using the standard depth to pressure equation [17]. Modern CTD systems achieve salinity accuracies better than ±0.005 PSU, with some instruments like the Sea-Bird 911 Plus demonstrating historical accuracies of ±0.002 PSU or ±0.0002 PSU [17] [18].

2.4.4   Applications and Limitations

Conductivity-based salinity measurements excel in most oceanographic and water quality applications due to its accuracy, speed, and reliability. The conductivity method allows for real-time data capture, continuous monitoring, and easy integration with autonomous devices [19].

However, this method does face some limitations. Due to its dependance on the water's capacity to conduct electricity, freshawater applications require specialised low-conductivity sensors, while hyper-saline environments could exceed the standard calibration range. The method's reliance on emperical correlations derived from typical seawater compositions can introduce errors in waters ocean waters affected by external factors such as pollution

or freshwater inflow from connecting rivers, which can alter ionic composition and introduce variability not captured by standard seawater-based calibrations. In such environments supplementry practices may be necessary for accurate salinity measurements [20].

2.5 Machine Learning Applications in Electrochemical Impedance Spectroscopy

2.5.1 EIS

Electrochemical Impedance Spectroscopy (EIS) is an analytical technique used to characterise the electrical properties of materials and interfaces, usually electrode or an electrolyte, by measuring impedance (opposition to current flow) across a range of frequencies [21]. In essence, EIS describes the electrode behavior in the presence of an electrolyte in terms of electrical parameters, including resistances and capacitances. It involves measuring the system's response to an applied electrical signal, and then transforming these time-domain signals into the frequency domain. The technique is based on applying an /glsac signal to the electrodes and determining the corresponding response. Unlike simple conductivity measurements that capture only resistive properties at a single frequency, EIS measures both the magnitude and phase of impedance across a range of frequencies, typically from 0.001 Hz to 1 MHz [22].

The complex impedance $Z(\omega) = Z'(\omega) + jZ''(\omega)$ contains both resistive (real) and reactive (imaginary) components, that respond differently to ionic concentration, species mobility, and electrode interface effects. High-frequency impedance primarily reflects bulk solution resistance, while lower frequencies reveal interfacial (between two faces) phenomena including double-layer capacitance and charge transfer resistance [23].

EIS has demonstrated success in quantitative concentration analysis across diverse solution systems. In electrolyte analysis, multi-frequency measurements enable determination of ionic strength through characteristic impedance signatures that are less sensitive to temperature variations and electrode fouling than DC conductivity measurements [22].

2.5.2   EIS Fundamentals

The EIS measuring process invloves applying an AC signal at a specific frequency and amplitude to a sample. By sweeping across a multitude of frequencies, a complete impedance spectrum can be obtained. The impedance magnitude $|Z|$ and phase angle ϕ at each frequency is recorded, and are used to analyse the electrical properties of the solution [23]. For salinity, it can be used to characterise the electrical properties of ionic solutions, including seawater, by analyzing how ions affect the impedance spectrum. This data can be used to approximate the system using Equivalent Electrical Circuits (EECs), which are circuits ussed to describe a system with discrete electrical circuit elements [22]. EECs fulfill the overall goal of EIS is to describe the behaviour of the electrode and solution in terms of electrical parameters such as resistances and capacitances [21].

2.5.3   Limitations of Traditional Equivalent Circuit Modelling

Traditional impedance analysis relies on the modelling of EECs, to derive the salinity from the impedance. This process requires extensive electrochemical expertise, in order to understand the chemical composition of the solution. Manual parameter extraction from impedance spectra is time consuming and may fail to capture subtle features that correlate with salinity. Linear calibration methods assume simple relationships between impedance measurements and concentration, which may not hold across wide salinity ranges or in solutions with varying ionic compositions. Temperature effects and electrode aging can further complicate traditional calibration approaches [22].

2.5.4   Machine Learning Modelling for Impedance Analysis

Machine learning approaches offer advantages by learning complex non-linear relationships directly from experimental data without the need for explicit physical models or EECs. Supervised learning algorithms can map measured impedance values at specific input signal frequencies and amplitudes to target salinity concentrations through automated pattern recognition. The general framework involves training a model on a dataset of known salinity samples, where each sample is characterised by its impedance response to AC excitation at defined frequencies and amplitudes [24]. The trained model can then predict salinity from new impedance measurements, effectively learning the impedance-salinity mapping function. Machine learning eliminates subjective bias inherent in manual

impedance interpretation and consistently applies identical analysis procedures across all measurements. The algorithms can identify complex patterns in multi-frequency impedance data that may be overlooked in traditional analysis [25].

2.5.5 Machine Learning Algorithms for Salinity Prediction

Neural Networks

Neural networks are machine learning programs that make decisions similarly to the human brain, using processes that mimic how biological neurons work together to identify patterns, weigh options, and reach conclusions [26].

Every neural network consists of layers of nodes (artificial neurons), these being an input layer, one or more hidden layers, and an output layer. Each node connects to others and has its own weight and threshold value. When a node's output exceeds its threshold value, it activates and sends data to the next layer, if not, no data passes through. This creates a feed-forward process where information flows from input to output. Each node functions like a linear regression model with inputs, weights, a bias, and an output. Weights determine how important each input is, with larger weights having greater significance. Inputs are multiplied by their weights, summed together, and passed through an activation function to determine if the node fires. Neural networks rely on training data to learn and improve accuracy over time. They use cost functions to evaluate accuracy and adjust their weights and biases through gradient descent and backpropagation to minimize errors and reach optimal performance [26].

Artificial Neural Networks (ANNs) represent the most widely adopted machine learning approach for impedance-based concentration prediction due to their exceptional capability for modelling complex non-linear relationships. The architecture typically consists of an input layer receiving impedance features such as frequency and phase, one or more hidden layers that extract relevant patterns, and an output layer producing predictions [27]. Hidden layers with non-linear activation functions enable the network to capture complex impedance-salinity relationships [28].

Deep neural networks with multiple hidden layers can learn hierarchical representations, potentially identifying frequency dependent patterns at different levels. However, they require larger training datasets and careful regularisation to prevent overfitting [28].

Random Forrest Algorithms

Random forest is a machine learning algorithm which combines the output of multiple decision trees to reach a single result. It handles both classification and regression problems. The model is built from multiple decision trees. Decision trees start with a basic question and use a series of questions (decision nodes) to split data, ultimately leading to a final decision at the leaf node. They're trained through the Classification and Regression Tree (CART) algorithm. Unlike single decision trees that can be prone to bias and overfitting, when multiple uncorrelated decision trees form an ensemble in random forest, they predict more accurate results. By accounting for potential variability in the data through feature randomness, random forests reduce the risk of overfitting, bias, and overall variance, resulting in more precise predictions [29].

Random Forest methods demonstrate excellent performance with mixed data types, enabling simultaneous utilisation of raw impedance values, derived electrochemical parameters, and statistical features within unified prediction models. The algorithm's resistance to overfitting makes it particularly suitable for limited training data scenarios common in analytical applications [30].

Chapter 3

Methodology

3.1 Salinity Measurement Method

A CTD sensor, which measures salinity using conductivity, temperature and depth, was chosen as the salinity measurement device. When choosing a measurement technique multiple factors needed to be considered. Firstly, the salinity measurements are to be conducted in the Antarctic, where the environment, and remote nature of the area, make majority of the measurement methods unusable. Secondly, the device would need to fit through an ice core hole with a diameter of $100mm$, and lastly, the device would need to be able to take continuous measurements.

CTD sensors do not require sample collection, unlike chlorinity titration, gravimetric analysis and refractometry. This removes both the need for sample collection and the challenges of sample degradation, storage and transport logistics.

Modern CTD sensors are compact, and can easily be designed for specific space constraints. This coupled with its deployments flexibility make it the preferred choice over methods, such as laboratory methods, which suffer from deployment constraints. CTD sensors allow for continuous realtime monitoring, a characteristic none of the the alternative methods provide. The alternative methods either require sample collection, or cannot measure continuously.

CTD instruments inherently measure conductivity, temperature and pressure simultaneously, providing salinity measurements with temperature and depth compensation, whereas laboratory methods measure salinity only, and require seperate temperature measurements.

These factors coupled with the researcher's significant experience with PCB design and electronics influenced the choice for a CTD sensor.

3.2 Electrode Design

When measuring conductivity, choosing an electrode material plays a significant role in the accuracy of the measurements. To get an accurate measurement of the resistance of the water, ideally, a electrode resistance of zero is required. This would allow the resistance measurement to be entirely due to the resistance of the water. Most conductive materials have conductivities of order $10^6 - 10^8 S/m$, which is negligible compared to sea (salt) water, which has an average conductivity of $3.31 S/m$ [31][32]. Preferably, the material with the highest conductivity, silver, would be used. However, conductivity is not the only factor considred when designing an electrode. The electrodes will be submerged in saltwater, which is highly corrosive. The material chosen will require high corrosive resistance. Silver, though having the highest conductivity, has a low corrosion resistance, and therefore cannot be used in this application [33].

Titanium is the material of choice for ocean-use [34]. It is essentially corrosion-free, and offers a conductivity of 2.68×10^6 [31]. However, titanium is expensive and fell out of the budget of this project. Gold boasts both a high conductivity of 4.10×10^7, higher than titanium but lower than silver, and a high corrosion resistance, making it an ideal choice. Gold is also a commonly used material in electronic design, with it being used in Printed Circuit Board (PCB) manufacturing, to protect copper pads from corrosion. This is done through a Electroless Nickel Immersion Gold (ENIG) plating process, where a layer of nickel is chemically deposited onto the exposed copper traces, to prevent the copper from oxidizing, and then a layer of gold is applied over the nickel through an emmersion process, to protect the nickel. This process is significantly more expensive compared to standard PCB manufacturing, however, it allowed for the use of gold electrodes, and therefore was factored into the budget.

In order to utilise the ENIG process a PCB was used to design the gold electrodes. This allowed the electrodes to be designed with a known area and seperation distance, allowing for accurate conductivity calculations. A solder pad was used to design the portion of the PCB that would act as the electrode, since it allowed the copper/gold to be exposed. Then during manufacturing ENIG was chosen as the surface finish, to achieve the gold finish.

The PCB was designed to allow for easy calculation of the conductivity σ, using the equation below:

$$\sigma = \frac{L}{RA} \tag{3.1}$$

where L is the distance between the electrodes, R is the resistance of the water, and A is the cross-sectional area of the electrodes. A square face of $20mm \times 20mm$ was chosen to allow for easy cross-sectional area calculations, and a distance of $10mm$ was chosen as the seperation distance. This distance was chosen as it is close enough to reduce current spreading, but not too small to where the water could not flow easily between the electrodes. A $2mm$ fringe guard was added around the main electrode area to reduce current fringing, which is an effect that causes the current to spread beyond the edges of the gap [35]. The fringe guards counteract this by saturating the area surrounding the main pads with current, preventing them from fringing.

The resistance of the electrodes was calculated using the Equation 3.1 and was found to have an approximate resistance of 7.55Ω

The electrode PCB was designed with the consideration of mounting to the probe PCB. To accomodate this, solder pads were added to allow the electrodes to be soldered to the probe PCB. Mounting legs were also factored into the design to ensure that the electrodes stayed straight and secure. The design can be seen in Figure 3.1.
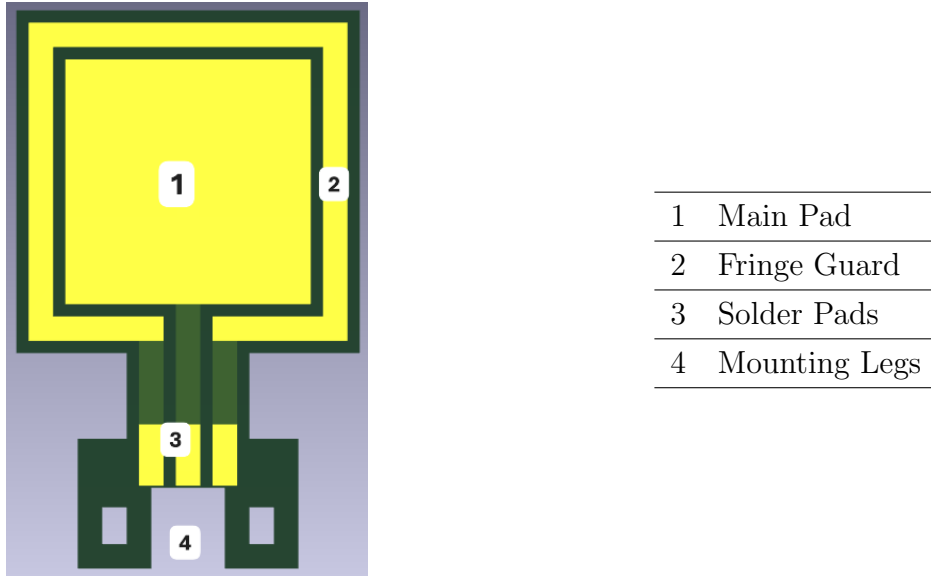

1	Main Pad
2	Fringe Guard
3	Solder Pads
4	Mounting Legs

Figure 3.1: Gold Electrode PCB

3.3   Resistance Measurement

There are multiple ways to measure resistance, however most rely on the same principle, which is the voltage divider principle. This principle works by using a series circuit with two resistors, and a constant known input voltage. The voltage over each of the resistors will be proportional to their resistance, and therefore, if the resistance of one resistor is known, the resistance of the other can be calculated. A simple voltage divider circuit can be seen in Figure 3.2. For this application the electrodes were chosen as the R_2 resistor, with R_1 being a large resistor of known resistance.
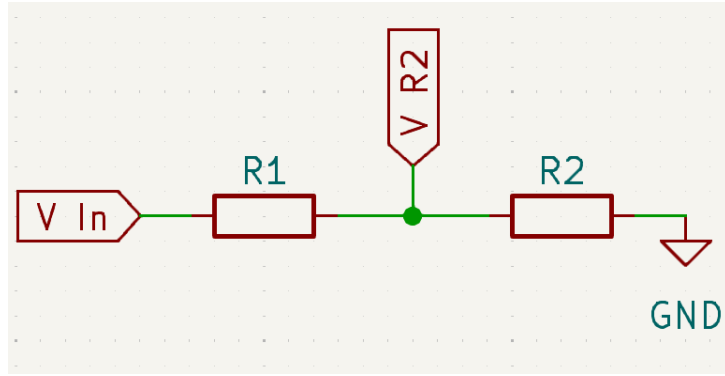

Figure 3.2: Simple voltage divider circuit used for resistance measurement.

Equations 3.2 and 3.3 are used to calculate the resistance from the voltage divider equation.

$$V_{R2} = V_{In} \times \frac{R_2}{R_1 + R_2} \tag{3.2}$$

$$R_2 = \frac{R_1 \times V_{R2}}{V_{In} - V_{R2}} \tag{3.3}$$

3.4   Circuit Design

The probe circuit is the circuit which contains the resistor divider, was designed to be printed onto a PCB. This design was influenced by Reference [36], where a similar device was designed for salinity measurements in ice columns. A PCB was chosen for this circuit as the researcher had significant experience with PCB design, and the manufacturing process offered higher precision than hand soldering, and is relatively cost-effective. Significant improvements and modifications were made to the resistor divider circuit, to allow for a wider range of testing.

For input power, a Digital to Analogue Converter (DAC) was used to drive the circuit. This allowed to the input voltage to be varied between $0V$ and the referencevoltage, which was chosen to be $5V$. This allowed for a range of voltages to be applied, which allowed for the measurement of the water's voltage-resistance relationship, and the creation of AC signals. A function generator was considered for generating the AC signal, as it would allow for signals of a wider frequency and and high precision, however the price could not be accomodated by the budget. The choice of DAC, and all following components, was first influenced by availability on JLCPCB, the PCB manufacturing house. The MCP4725 was chosen for its high resolution of 12-bits, offering a digital range of 0-4095, fast update time of $6\mu s$, and interface speed of 3.4MHz. These features allow for both DC and AC signal analysis.

An op-amp with unity gain was the connected to the output of the DAC. This is because DACs have limited output drive capabilities, and the op-amp would allow for heavier loads to be driven. Additionally the op-amp offers improved output stability, introduces impedance isolation, which protects the DAC from load variations and feedback effects, and allows for better sine wave quality.

As mentioned in Section 3.3, for the resistor divider circuit, the electrodes would serve as R_2 and a known resistor as R_1. Three alernative values of R_1 were chosen, to accomodate for any circuit errors. These could be switched between using the TS3A4751 multiplexer Integrated Circuit (IC). This switching multiplexer was chosen, for its low on-state resistance of 0.9Ω, and fast switching speed of $4 - 5ns$ [36].

The R_1 resistor values were chosen to be 100Ω, $1K\Omega$ and $10K\Omega$. These values would be used when the resistance between the probes was $1 - 10\Omega$, $10 - 100\Omega$, and $100 - 1K\Omega$ respectively. Each IC contained 4 switches.

For measuring the output resistor, the voltage over it was directed into a multiplying op-amp with a gain of 11. This increases the resolution for the Analogue to Digital Converter (ADC) readings, as low voltages may be hard to differentiate between when converted to digital data.

This configuration would allow for a minumum resolution of 11% of V_{DAC} and maximum of 100% of V_{DAC}, for the voltage measurement by the ADC, as shown in Equations 3.4 and 3.5 [36]. Equations 3.4 and 3.5 show for the expected resistance of 7.55Ω falling into the $1 - 10\Omega$ range. However, if the resistance falls into the $10 - 100\Omega$, or $100 - 1K\Omega$, the respective R_1 resistors would be used and the maximum and minimum DAC resolutions would be the same.

$$\frac{1\Omega}{1\Omega + 100\Omega} \times V_{DAC} \times 11 = 11\% V_{DAC} \tag{3.4}$$

$$\frac{10\Omega}{10\Omega + 100\Omega} \times V_{DAC} \times 11 = 100\% V_{DAC} \tag{3.5}$$

The accuarcy of the R_1 resistor is integral to acheiving an accurate R_2 measurement. The resistors available on JLCPCB had an acurracy of $\pm 1\%$. To increase the accuracy 3 equal resistors were put in parallel. This decreases the uncertainty of the total equivalent resistance [36]. This is shown in Equations 3.6 to 3.9.

$$R_T = \left[\sum_{i=1}^{n} \frac{1}{R_n} \right]^{-1} \tag{3.6}$$

If all the Resistors are equal this simplifies to:

$$R_T = (\frac{n}{R})^{-1} = \frac{1}{n} \times R \tag{3.7}$$

To propogate uncertainty the standard equation for combined uncertainty can be used:

If a quantity y depends on several independent variables $x_1, x_2, \ldots, x_n$:

$y = f(x_1, x_2, ..., x_n)$

and each x_i has a standard uncertainty $u(x_i)$ then the combined standard uncertainty of y, denoted $u_c(y)$, is:

$$\delta_y = \sqrt{\sum_{i=1}^{n} \left(\frac{\partial f}{\partial x_i} \delta_{x_i} \right)^2} \tag{3.8}$$

For Resistance this can be shown as:

$$\delta_{R_T} = \sqrt{\sum_{i=1}^{n} \left(\frac{\partial R_T}{\partial R} \delta_R \right)^2} = \sqrt{\left(\frac{1}{n} \delta_R \right)^2} = \frac{1}{n} \delta_R \tag{3.9}$$

Using the above equations, with resistors with an individual uncertainty of $\pm 1\%$, three

resistors in parallel have a combined uncertainty of $\pm 0.33\%$ To created the intended R_1 resistances of 100Ω, $1K\Omega$ and $10K\Omega$, the three parallel resistors were chosen to use values of 300Ω, $3K\Omega$ and $30K\Omega$ respectively.

A second switch circuit was then used to configure the R_2 resistor. With there being two electrodes, the switching circuit allowed for the user to choose which would be the anode and the cathode. The switch also included a calibration resistor of 5Ω, which would allow for the calculation of the gain of the ADC when measuring. This calibration resistor was also created using a parallel resistor configuration, where four 20Ω resistors were connected in parallel to give the require resistance at an uncertainty of $\pm 0.25\%$.

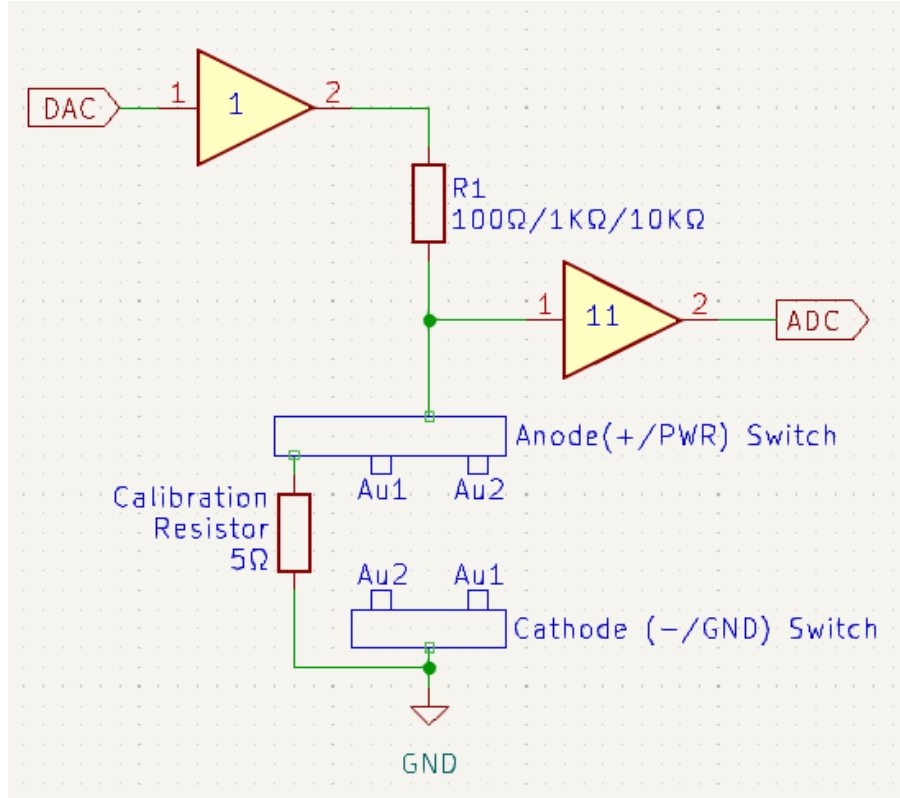A simplified circuit diagram showing the resistance measuring circuit is shown in Figure 3.3.

Figure 3.3: Simple circuit diagram of the resistance measuring circuit.
Note: Au1 Denotes Gold Electrode 1, and Au2 Gold electrode 2.

A third switch was added to allow for the configuration of the fringe guard, allowing the fringe guard paired with an electrode to share the same voltage configuration, i.e. when an electrode acted as the anode its fringe guard would also act as an anode, and vice versa. The voltage of R_1 was directed through a unity gain buffer op-amp, and then connected on its output to the fringe guard, allowing for the same voltage over the electrodes to be

over the fringe guards without affecting the measurement of the electrode voltage.

Four points on the resistance circuit were routed to seperate ADCs, and a test point added to allow for the comparison between the voltage measured by the ADC and by a multimeter. These points were at the DAC output before the unity gain buffer op-amp, after the unity gain buffer op amp, before the 11x multiplying op-amp and after the 11x multiplying op-amp. A seperate capacitor was connected across each of these points and ground to stabilise the ADC readings and remove noise. These capacitors were connected via switches, to allow them to be disconnected when an AC signal needed to be measured. Two additional test points were added to measure the rail voltages from the voltage regulators.

In addition to the resistance measuring circuitry, a waterproof pressure and temperature sensor was included, as these values are needed for calculating salinity. The MS583702BA01-50 was chosen for its low price and availability on JLCPCB. This sensor only allowed for up to 2 Bar pressure measurements, which was enough for this prototype, but would not satisfy the real-world requirements of the salinity probe. Lastly, an RS-485 IC was included for inter board communication.

A ESP-32 S2-Mini-2 was chosen for the microcontroller, as it was the most cost effective ESP32 based microcontroller. It offered an FPU, allowing for the complex salinity calculations to be done, did not require a Universal Asynchronous Receiver-Transmitter (UART) bridge as it has built-in USB OTG support, allowing it to connect directly to a computer for easy programming, which was done via a USB-Micro port, and offered 13-bit ADCs, allowing for a good voltage measurement resolution. Additionally the wireless capabilities allowed for easy debugging, through a web interface, as the reasearcher's computer only had one USB port. The researcher also had significant experience with this microcontroller.

A controller PCB was designed alongside the probe PCB. This controller was designed to communicate with the probe while it was submerged, sending it instructions and receiving results. It allowed for the measurements to be recorded in a *.txt* file on a micro-SD card, and displayed on a 16×2 LCD screen. The PCB for this controller was minimal, and relied on external breakout circuit boards. This was due to budget constraints, and did not affect the effectiveness of the controller. Only the voltage regualtion circuitry, and inter-board communication (RS-485) circuitry were included in the production. Headers were included on the controller PCB to allow an ESP-Wroom-32 Devkit moduleto be mounted to it. Additional headers were included to allow the breakout boards for the LCD display and SD card reader to connect to the ESP32.

For the inter-board connection the RS-485 communication protocol was chosen. The ESP32 microcontrollers do support wireless communication through bluetooth and Wi-Fi. However, wireless communication, especially electro-magnetic waves suffer interference [37]. A wired connection medium, the RS-485 protocol was chosen. Compared to most other communication protocols which typically support distances no longer than $\pm 50m$, RS-485 supports up to 1200m, and has good underwater stability. The IC only requires simple I^2C and is relatively cheap. RS-485 usually uses a pair of twisted cables, which strengthens the electromagnetic magnetic interference rejection and reduces signal degradation. However, due to availability, simple 4-core communication was used, where the additional two cores were used to transmit power between the PCBs.

3.5   Assembly and Programming

3.5.1   PCB and Circuit Assembly

The Probe, Controller and electrode circuirty PCBs were designed using KiCAD software, and manufactured by JLCPCB. The KiCAD design files for these can be found in the GitHub repository linked in Appendix C.

The probe PCB had dimensions of 50×50mm and was fabricated onto a 4-layer PCB. This was chosen as the probe would need to fit in the ice hole with a diameter of 100mm, and JLCPCB offeres a discounted rate on 4-layer PCBs if the dimensions are 50×50mm or less. This size also made debugging easier. In addition to the components required for transmission and measurement, test points with headers were added for easy debugging, and an indicator Light Emitting Diode (LED), to indicate power. The probe is shown in Figure 3.4.

The controller was relatively simple, and only require a 2-layer PCB, with dimensions of $70 \times 55mm$. This size and layer count fell into the same discounted bracket as the probe PCB. The external micro-SD card reader was connected to the PCB through a breadboard. The chosen ESP32-Wroom Devkit module when designing the PCB was not the same one the researcher had access to when assembling the controller, and differed in size. To accomodate for this the available ESP32-Wroom module was also placed on the breadboard and was connected to the PCB via jumper cables. Additionally the 16x2 LCD display was not used because of this. The complete Controller PCB and additional circuitry can be seen in Figure 3.5.
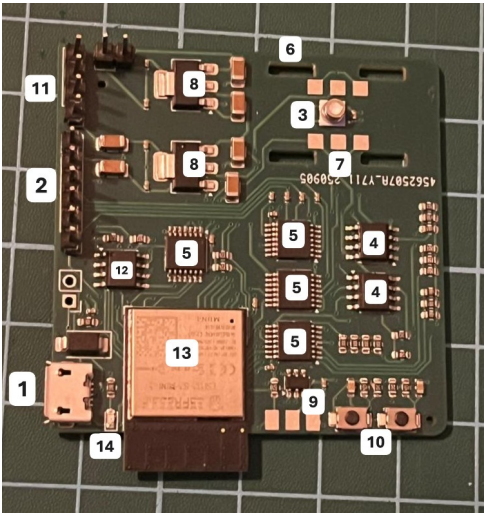
1	USB-Micro Port
2	Test Points
3	Pressure Sensor
4	Op-Amps
5	Switch ICs
6	Gold Electrode Mounts
7	Gold Electrode Solder Pads
8	Voltage Regulators
9	DAC
10	Boot and Enable Buttons
11	RS-485 Port
12	RS-485 IC
13	ESP32 Microcontroller
14	Power Indicator LED

Figure 3.4: The probe PCB
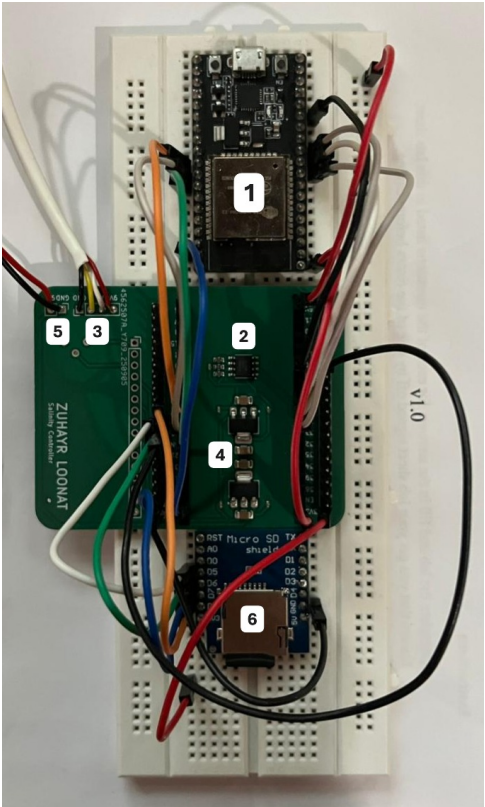
1	ESP32-Wroom-Devkit
2	RS-485 IC
3	RS-485 Port
4	Voltage Regulators
5	Input Power
6	Micro-SD Card Reader

Figure 3.5: Controller PCB and Additional Circuitry

The two PCBs were connected via 4-core communication cable, with pins for RS-485 Tx and Rx, Ground and 9V Power. Additionally, 6 core wire was connected to the probe PCB along the 6 test points, to allow for easy debugging when submerged. Both PCBs were powered by an input voltage of 9V which was stepped down appropriately, using voltage regulator ICs, for a stable power input.

The electrode manufacturing was simple, as it consisted of the gold plated solder pads, as mentioned in Section 3.2. No additional modifications had to be made to the electrode PCBs, and they were hand soldered to the corresponding solder pads on the probe PCB.

3.5.2 Waterproofing

Since the probe PCB would need to be submerged in water, it will would need to waterproofed. A multitude of methods were considered including conformal coating, a 3D-printed waterproof enclosure, and resin casting. Conformal coating is a thin proctective layer applied to shield circuitry and PCBs from moisture and extreme temperature, and usually comes in a spary can. It is relatively cheap but has a low pressure resistance, and offers low physical protection. A 3D-printed enclosure was considered too complex, ultimately leaving a resin cast as the chosen method. This method offers good physical protection and is considered the most reliable.

The RE33/HE33 resin from AMT Composites was chosen for the PCB to be cast in, as it is specifically designed for the encapsulation of electrical components. The cast was made using acrylic sheeting, which were chosen because they do not stick to the resin. The sheets were cut using a hack saw and joined using waterproof superglue.

The electrodes were spaced using two pieces of acrylic measured to 10mm (i.e. the electrode seperation distance). A plastic straw was used to isolate the pressure sensor as the diamter of the stray matched the pressure sensor perfectly. This ensured that the sensor could measure the pressure of the water accurately. The required cables were soldered to the PCB before pouring the resin. A fully encapsulated probe PCB can be seen in Figure 3.6.
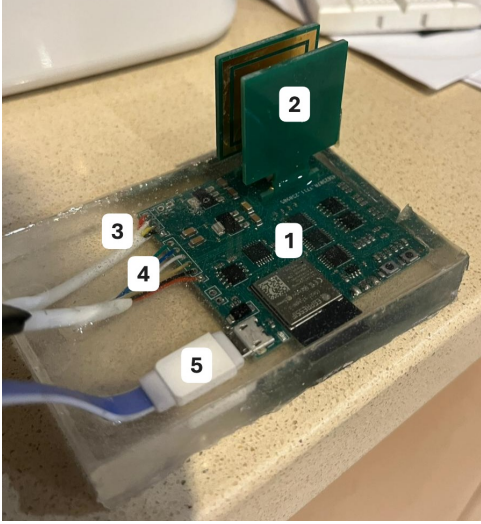
1	Probe Board
2	Gold Electrodes
3	RS-485 and Power Cable
4	Test Point Cable
5	Programming Cable

Figure 3.6: Encapsulated Probe

3.5.3   Microcontroller Programming

The controller was programmed to send commands to the probe via RS-485, and the probe to follow the command and return the data back to the controller. These commands would first be sent by a computer to the serial monitor on the controller board, and then would be sent from the controller to the probe. Multiple measurement modes were programmed into the probe board and they were trigered with specific commands. A seperate C++ header file, with functions for the salinity calculation equations, mentioned in Section 2.4.2, was created for ease of coding and and reusability.

The voltage measurements were done using the ESP32's built in ADCs, which used a reference voltage of $3.3V$. To account for measurement inaccuracies caused by the DAC, ADC or op-amp, the calibration resistor was used to find a calibration factor, which will be denoted by C_F. This factor was calculated by connecting the calibration resistor (R_2) to a chosen R_1 resistor, and measuring the voltage drop over it. This value would then be compared to the expected voltage drop, calculated mathematically. The expected voltage is divided by the measured voltage to give the calibration factor C_F. Readings from the ADC would then be multiplied by this calibration factor, removing any inaccuracies. The calculation of the calibration factor is shown in Equations 3.10 to 3.13.

$$\text{Given calibration resistor } R_C = 5\Omega \tag{3.10}$$

$$\text{Expected } V_C = 11 \times V_{IN} \times \frac{R_C}{R_C + R_1} \tag{3.11}$$

$$\text{Meausured } V_C = \frac{\text{ADC Reading}}{\text{ADC Resolution}} \times V_{Ref} \tag{3.12}$$

$$\text{Calibration Factor } C_F = \frac{\text{Expected } V_C}{\text{Meausured } V_C} \tag{3.13}$$

Measurement modes were created for calibration testing, DC analysis and AC analysis. For all these modes voltage measurements using the ADCs were taken before the unity gain buffer op-amp, after the unity gain buffer op amp, before the 11x multiplying op-amp and after the 11x multiplying op-amp. Additionally temperature and pressure readings were taken for all modes, to allow for corrections. All salinity calculations were calculated using the PSS-78 equations mentioned in Section 2.4.2.

Calibration Test

The calibration test function was designed to measure the inaccuracies of the ADCs, DAC and op-amp, and to return a calibration factor based on these inaccuracies. It used Equations 3.10 to 3.13 to achieve this.

DC Voltage Sweep

This procedure was designed to take voltage measurements over the probes through a range of voltages, were the fuction allowed for the maximum voltage, and chosen R_1 resistor, to inputted. The DAC would output a voltage, the calibration resistor would be measured to calculate the calibration factors for each ADC and then the electrode voltages would be measured bi-directionally (Au_1 as +, Au_2 as negative, and vice versa). This would be done for the full specified range of voltages in increments of $0.1V$.

A resistance would then be calculated for the corresponding voltage, and this would be used to calculate the conductivity. The conductivities and resistances for each volatage step would be returned as well as the temperature and pressure values. The average conductivity is also returned

DC Single Voltage

This function was designed to take a single voltage reading. Similar to the DC voltage sweep, this first measures over the calibration resistor, to find the calibration factor, and then takes bi-directional measurements over the electrodes. the voltage is then used to calculate the conductivity, which was returned with the temperature and pressure values.

The DC procedures were first to be done on the standard solution of 35 PSU at $15°C$, mentioned in Section 2.4.1. This allowed for the conductivity of the standard solution to be calculated, as the calculation of salinity relies on the ratio between the salinity of the standard solution and the sample solution.

AC Wave Generator

For EIS, AC signals are used. This function allowed for a frequency and amplitude to be inputted. It would then output a sinusoidal waveform using the DAC, and the output over the electrodes would be measured. This allowed for the values of the input and output waveform to be returned. For the duration of this function, the stabilising capacitors connected to the ADCs, mentioned in Section 3.4 were disconnected, as they would interfere with the AC signal.

The values for the input and output waves were exported to a *.csv* file and then processed in MATLAB and python.

Inter-Board Communication

As mentioned previously, the controller board was programmed to send instructions to the probe, and receive the readings for those functions, from the probe. Half-Duplex RS-485 was effectively used as only one board could communicate at a time. The probe board would be set by default to receive mode, and controller to transmit mode. The controller would send an instruction to the probe, and would then change to receive mode, awaiting the readings from the probe. Once the probe received the instruction it would change to transmit mode, allowing it to send the readings. Once the readings were sent, the probe would return to receive mode, and upon receiving the readings the controller would return to transmit mode. The controller instructions were typed in manually via the controller's serial monitor. Upon receiving the readings, the controller would display

them in the serial monitor and print them to the *.txt* file on the micro-SD card.

3.5.4 Machine Learning Programming and AC Analysis

For salinity prediction through EIS, impedance measurements over a range of input frequencies and amplitudes would need to be taken. This would allow the machine learning to be formatted as a regression task, where the input features consist of:

- AC exitation frequency (f)

- AC exitation amplitude (A)

- Measured impedance magnitude $|Z|$

- Measured phase angle (ϕ)

The output is the predicted salinity value. During the training the model learns the mapping function (function is denoted with m instead of f as f is used to represent frequency):

$$\text{Salinity} = m(f, A, |Z|, \phi) \tag{3.14}$$

Multiple input frequency-amplitude combinations can be used as input features, enabling the model to leverage information across the entire impedance spectrum for improved salinity accuracy [38].

For EIS salinity measurements, neural networks would theoretically be the superior choice [39]. This is due to their ability to model highly complex, non-linear relationships which are inherent in electro-chemical systems [40]. They have the ability to automatically learn feature interactions, without manual feature engineering and their ability to learn hierarchical representations makes them especially suited for EIS data [39]. However, given the constraint of a small sample size, random forest is the more practical and effective choice for this application. Random forests require significantly less training data to achieve reliable performance, often working well with just dozens to hundreds of samples rather than the thousands needed for neural networks. With limited data, neural networks are highly prone to overfitting, essentially memorising the training examples rather than learning generalisable patterns, which would result in poor performance on new salinity measurements [41]. Random forests mitigate this through their ensemble approach (using multiple smaller models), which reduces variance and improves robustness

even with small data sets. Additionally they require minimal parameter tuning and work reasonably well 'out of the box', whereas neural networks require extensive architecture design, learning rate optimisation, and regularisation techniques that become nearly impossible to properly tune without sufficient validation data [41].

Due to these factors random forrest was chosen. The programming for this model was done in python via a Jupyter Notebook, as this is widely used in the industry. First, to test the random forrest model, a Resistor-Capacitor dataset was used, This allowed for the evaluation of the accuracy of the model. It used an input frequency and amplitude and output impedance magnitude and phase, mapped to a dielectric permittivity (the other parameters for capacitance were the same for all capacitor values), to prepict permittivity of the capacitor, based on the inputs. Once the Resistor-Capacitor model was tested, the model was updated to support the EIS parameters for salinity.

To create the EIS dataset for the random forrest model, measurements of signals of varying frequency and amplitude, in solutions of varying salinity would be taken. It was planned to use 10 solutions of varying salinity, with frequencies 1-100Hz in increments of 20Hz, since the MCP4725 DAC outputted these reliably, and amplitude 0-1V in increments of 0.2V. This would give a total dataset of 360 data points, enough to train the random forrest on.

Chapter 4

Testing and Evaluation

To properly evaluate the system, multiple testing procedures were implemented. These started with first testing the accuarcy of individual components on the PCB, and then testing the probes ability to measure salinity, through voltage measurements relating to conductivity. Additionally, tests were done on the ML model programmed to map the salinity.

A summary of the tests and their outcomes can be seen in Table **??**.

4.1   Component and Equipment Testing

Before the probe could be used to measure salinity, the accuarcy of its components needed to be tested. These procedures were completed before the probe was encased in resin, as access to the circuitry was required.

4.1.1   Resistor Testing

For accurate electrode resistance to be measured, the the $R1$ parallel resistor combinations would need to be measured. As shown in Section 3.4, by calculation, the $R1$ resistors should have equivalent resistances of 100Ω, $1K\Omega$ and $10K\Omega$, with an uncertainty of $\pm0.33\%$. These were measured using the $KeysightTechnologiesU3401A$ multimeter, which had a resistance accuracy of 0.1%. This multimeter would be used for all subsequent

DC voltage measurements, and has a voltage accuracy of 0.02%. The multimeter probes had a resistance of 0.154Ω which was accounted for. The $R1$ resistors were measured and are shown in Table 4.1.

Theoretical R (Ω)	Meausured R (Ω)
$99.67 - 100.33$	99.888
$996.7 - 1003.3$	1000.146
$9967 - 10033$	10005.746

Table 4.1: Table of R_1 resistor measurements

The calibration resistor with an expected resistance of $5\Omega \pm 0.25\%$ was measured to have a resistance of 5.142Ω. Taking into account the probe resistance, the calibration resistor had a resistance of 4.988Ω.

4.1.2 DAC and ADC Accuracy

Both the accuracy of the DAC and ADC needed to be measured as these were used for the output and measurement, respectively.

The first test was done by programming the DAC to output from its minimum to maximum value. This would allow for the evaluation of the DACs output offset and gain to be measured. The ADCs were also used to measure the output of the DAC, and these measurements were compared relative to the voltage measured by the multimeter. Figure 4.1 shows the relationship between the voltage inputted to the DAC, and its output voltage, with the output measured on the multimeter. Note that the reference voltage of the DAC was measured to be $5.001V$.
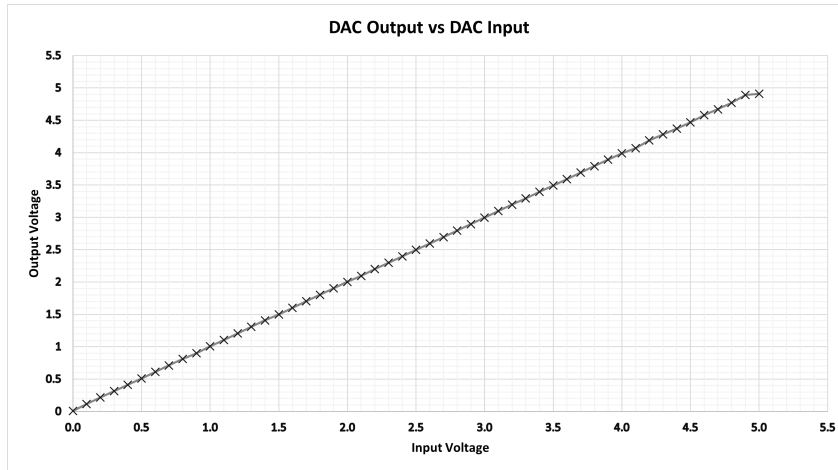
Figure 4.1: DAC Output Voltage vs Input Voltage

Based on the measurements made by the multimeter, the DAC had a output range of $0.0098V - 4.91V$, an offset of $0.0098V$ and gain of 0.98688.

The accuracy of the ADC was then tested by comparing the DAC output measured by the ADC and multimeter. Note, this ADC measurement was taken after the unity gain buffer op-amp. For this test, the ADC took 5 measurements at each voltage step, which were taken at $1\mu s$ interval. These 5 values were averaged to give the voltage at that step. The results of this test can be seen in Figure 4.2.
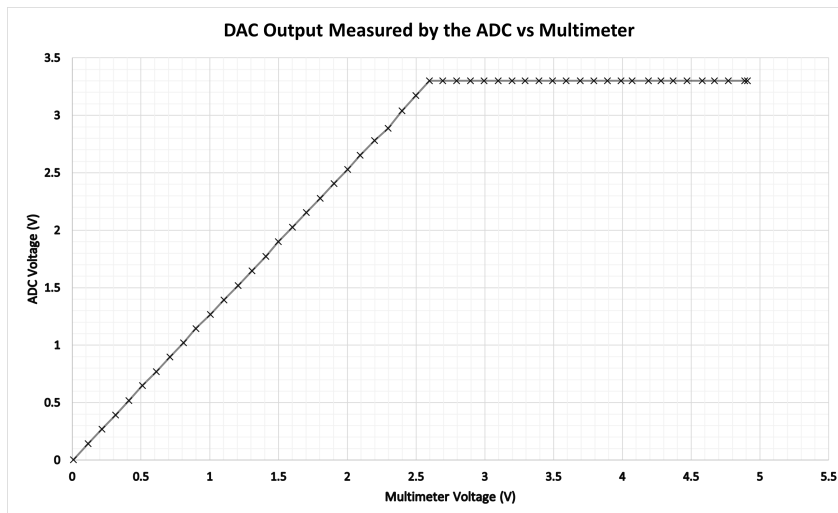

Figure 4.2: DAC Output Measured by the ADC vs Multimeter

Once the voltage measured by the ADC reaches $3.3V$ the ADC saturates as its reference voltage is $3.3V$. The gain of the ADC was calculated to be 1.28072 compared to the mulimeter.

4.1.3 Accuracy of Resistance Measuring Circuitry

In order to evaluate the resistance circuit's ability to accurately measure resistance, resistors were attached to the electrode's solder pads. This resistor acted as the $R2$ resistor and its value was calculated using Equation 3.3. The resistance was calculated using the voltage sweep and single voltage functions mentioned in Section 3.5.3 with some slight adjustments for calculating resistance only. These values were then compared to a multimeter measurement of the resistors, and the probe resistance taken into account. Resistances were measured at 0Ω, or a short circuit, and then $10 - 82\Omega$ using resistors from the E12-Series, with an accuracy of $\pm 5\%$ The 100Ω $R1$ resistor was used. The outcome of this test can be seen in Table 4.2.

Multimeter Resistance Ω	Measured R Ω	Acceptable Range Ω
0	0	0-0
9.848	9.99578925	9.5-10.5
11.972	12.0007881	11.4-12.6
15.124	15.0062442	14.25-15.75
18.872	18.1212224	17.1-18.9
22.004	22.0162646	20.9-23.1
27.101	26.9989572	25.65-28.35
33.012	33.0181212	31.35-34.65
39.201	39.0305398	37.05-40.95
47.100	47.0431559	44.65-49.35
56.023	56.0306769	53.2-58.8
68.014	68.0599057	64.6-71.4
79.785	78.208607	77.9-86.1

Table 4.2: Table for Resistor Measurement Test
Note 1: For this test an input of 2V was used
Note 2: Accepectable range indicates resistance values due to $\pm 5\%$ accuarcy

The voltage sweep test, from 0-2V, achieved a similar measuring accuracy as seen in Figure 4.3
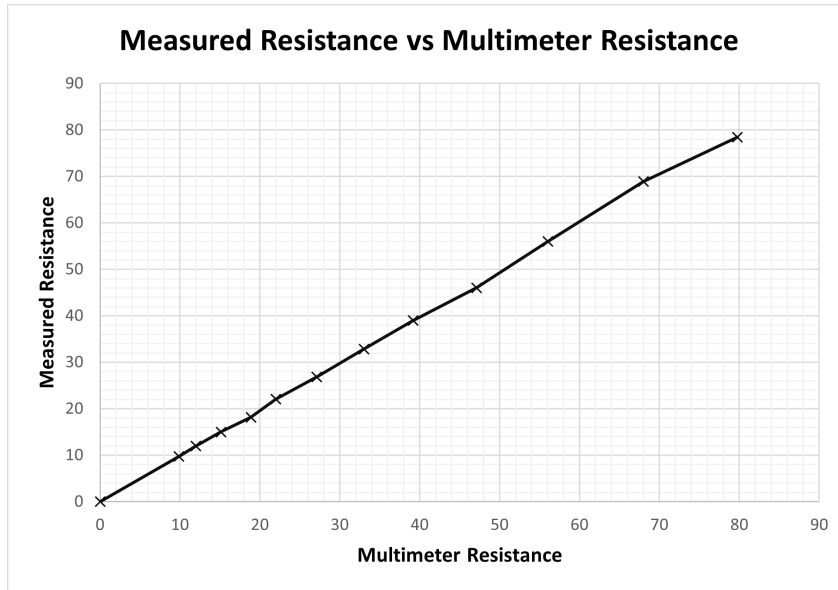
Figure 4.3: Resistance Measurement Test via Voltage Sweep

For both these tests, voltage calibration via the calibration resistor was done to ensure accurate voltage measurements.

4.2 Salinity Testing

In order for the probe to conduct salinity based tests, it was cast in epoxy as described in Section 3.5.2. Following this a range of tests were conducted, ranging from testing voltage measurements on saline solutions, to measuring salinity via conductivity.

4.2.1 Voltage Measurement Accuracy and Repeatability

In order to get an understanding of how the electrodes interact with saline solutions, a voltage sweep test was conducted multiple times with the same solution. This was done using the voltage sweep function, mentioned in Section 3.5.3, with some alterations, allowing for the function to return the raw voltage instead of the conductivity. The results showed that on the same solution, the the voltage sweep had the same effects. However, it was noticed that when a volatge reading was taken in quick succession to another there was a slight interference was caused by the water, to counteract this a 1 second delay was introduced between each measurement. After this delay was added, the interference was

no longer observed.

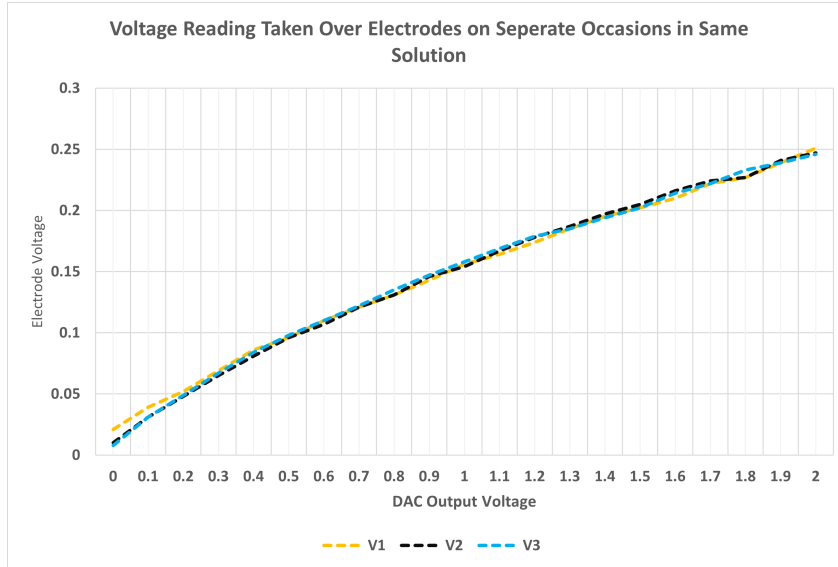Figure 4.4 shows voltage sweeps across the same solution on three seperate occasions.

Figure 4.4: Repeatability Test Results

4.2.2 Conductivity and Salinity Measurement

Obtaining Conductivity of the Standard Solution

For the measurement of salinity from conductivity, the conductivity of the standard solution of 35 PSU at $15°C$ and $0dbar$ must first be obtained. To evaluate this, both the voltage sweep and single voltage measurements wer taken in a solution at standard conditions. To achieve these conditions salt was mied into water until the salinity was 34.8 PSU. This value was used, as creating a solution of a specific salinity is a time-consuming process, and it was considered close enough for this experiment. To achieve a temperature of 15°C the water was cooled in a fridge to 4°C and then left out until it reached 15°C. The salinity was measured using a salinometer. Once the required conditions were achieved, a voltage sweep from $0 - 2V$ was done using the previously mentioned voltage sweep function. As mentioned in Section 3.5.3, in the voltage sweep description, this returns the conductivity and resistance for each step. All measurements for this and subsequent tests were conducted at $0dbar$, while using the 100Ω R_1 resistor as the measured resistances were between $1 - 15\Omega$. The sweep was conducted twice to ensure repeatability. From this test the average conductivity of the standard solution was found to be $3.53S/m$, with an average electrode/water resistance of 6.81Ω.

Similar results were obtained using single voltage measurements, where multiple readings were taken at one voltage using the DC Single Voltage function, and this was done for voltages of $1 - 1.5V$. Here the average resistance was calculated to be 7.39Ω and average conductivity of $3.53S/m$. These values correlate well with the expected resistance of 7.55Ω.

The Single Voltage Test can be seen in Table 4.3, with a graph illustrating the Voltage vs Resistance, taken from the Voltage Sweep Test, shown in Figure 4.5.

V IN (V)	Vp AMP (V)	Calib F	Probe V (V)	Resistance (Ω)	Conductivity (mS/cm)
1.2	1.112	0.7786	0.078709382	7.0195345	3.561489724
1.2	0.721	0.7786	0.051033691	4.4417047	3.628469589
1.3	1.355	0.7739	0.095330409	7.9130471	3.159195482
1.3	1.251	0.7739	0.088013536	7.2619240	3.442613812
1.4	1.312	0.7739	0.092305164	7.0586150	3.541770538
1.4	1.452	0.7739	0.102154800	7.8711082	3.176172238
1.5	1.573	0.7745	0.110753500	7.9721993	3.135897151
1.5	1.359	0.7745	0.095685955	6.8137148	3.669007482
1.6	2.211	0.7724	0.155525240	10.745988	3.226447904
1.6	1.451	0.7724	0.101886582	6.8009925	3.675934042
Mean				**7.38991**	**3.531706371**

Table 4.3: Table for Standard Salinity Solution Test
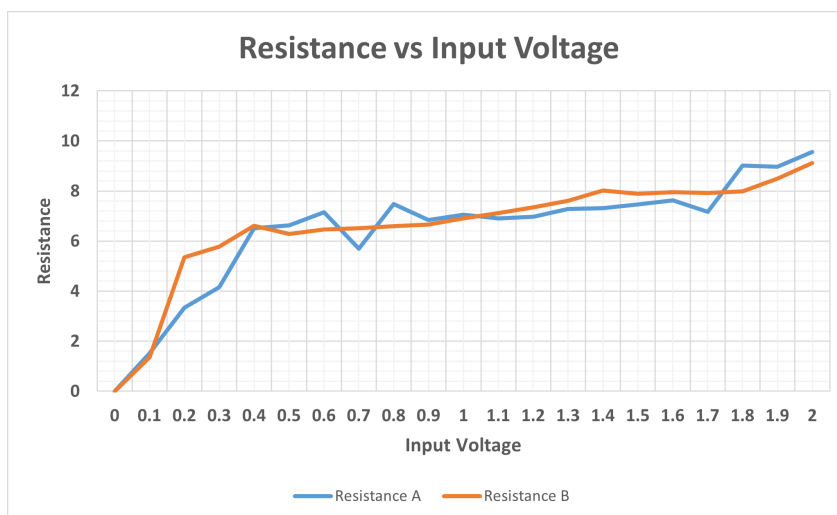*Note: For this test an R1 resistance of 100Ω was used.*

Figure 4.5: Volatge Sweep Test Showing Resistance vs Input Voltage

Measuring Salinity of Sample Solutions

Once the conductivity of the standard solution was found, the PSS-78 salinity equations could be used to find the salinity of sample solutions. The both the DC Single Voltage and DC Sweep Voltage functions were updated to return the salinity of a measured solution. For the DC Single Voltage Test, a voltage of $1.4V$ was found to return the most accurate value. Using these methods salinity of solutions were tested against a salinometer and compared. The comparisons for the Single Voltage test can be seen in Table 4.4.

Salinity (PSU)	T (°C)	Probe Voltage	Calib Factor	Corrected Voltage	Resistance (Ω)	Calculated Salinity
34.8	15	0.119	0.7739	0.0920941	7.041339901	35
30.1	15	0.145	0.7745	0.1123025	8.721186459	28.02
23.74	15	0.188	0.7601	0.1428988	11.36732667	20.71
23.72	24.31	0.108	0.7687	0.0830196	6.30378402	25.82
32.65	24.27	0.084	0.7693	0.0646212	4.839166235	35.15
15.8	20	0.197	0.7772	0.1531084	12.27920695	14.95
20.4	20	0.163	0.7779	0.1267977	9.958959389	18.75
17.26	20	0.197	0.7799	0.1536403	12.32712354	14.83

Table 4.4: Table for Sample Salinity Test

Note: T denotes temperature, Calib Factor denotes Calibration Factor.

From these measured values it can be seen that the probe has a measuring accuracy of approximately ±3.5 PSU.

4.3   EIS and Machine Learning

Chapter 5

Conclusions

These are the conclusions from the investivation and how the investigation changes things in this field or contributes to current knowledge...

Draw suitable and intelligent conclusions from your results and subsequent discussion.

Chapter 6

Recommendations

Make sensible recommendations for further work.

Bibliography

[1] R. H. Stewart, "Introduction to Physical Oceanography," 2008. Publisher: Robert H. Stewart.

[2] UNESCO, "Tenth report of the joint panel on oceanographic tables and standards," *UNESCO Technical Papers in Marine Science*, vol. 36, pp. 1–25, 1981.

[3] E. Lewis, "The practical salinity scale 1978 and its antecedents," *IEEE Journal of Oceanic Engineering*, vol. 5, pp. 3–8, Jan. 1980.

[4] F. J. Millero, *Chemical Oceanography*. Boca Raton: CRC Press, 4 ed., 2013.

[5] The Globe Program, "Salinity Protocol Using a Hydrometer."

[6] B. Kjerfve, "Measurement and analysis of water current, temperature, salinity and density.," *Estuarine hydrography and sedimentation*, vol. 1, no. 7, pp. 186–227, 1979.

[7] R. C. Millard and G. Seaver, "An index of refraction algorithm for seawater over temperature, pressure, salinity, density, and wavelength," *Deep Sea Research Part A. Oceanographic Research Papers*, vol. 37, pp. 1909–1926, Dec. 1990.

[8] D. Malardé, Z. Y. Wu, P. Grosso, J.-L. De Bougrenet De La Tocnaye, and M. Le Menn, "High-resolution and compact refractometer for salinity measurements," *Measurement Science and Technology*, vol. 20, p. 015204, Jan. 2009.

[9] Y. Zhang, L. Yuan, X. Lan, A. Kaur, J. Huang, and H. Xiao, "High-temperature fiber-optic Fabry–Perot interferometric pressure sensor fabricated by femtosecond laser," *Optics Letters*, vol. 38, pp. 4609–4612, Nov. 2013. Publisher: Optica Publishing Group.

[10] J. Abele, "The physical background to freezing point osmometry and its medical-biological applications," *The American journal of medical electronics*, vol. 2, pp. 32–41, Jan. 1963.

[11] "Freezing Point Depression Theory."

[12] V. Rana, P. Kumar, S. Banerjee, and A. Biswas, "Magnetic susceptibility investigation of the saline water intrusion problem: The LAMP-BHU protocol," *Journal of Earth System Science*, vol. 130, p. 140, July 2021.

[13] "Ion Chromatography."

[14] N. Gros, M. F. Camões, C. Oliveira, and M. C. R. Silva, "Ionic composition of seawaters and derived saline solutions determined by ion chromatography and its relation to other water quality parameters," *Journal of Chromatography A*, vol. 1210, pp. 92–98, Nov. 2008.

[15] E. L. Lewis and R. G. Perkin, "Salinity: Its definition and calculation," *Journal of Geophysical Research: Oceans*, vol. 83, no. C1, pp. 466–478, 1978. _eprint: https://agupubs.onlinelibrary.wiley.com/doi/pdf/10.1029/JC083iC01p00466.

[16] International Oceanographic Commission,, "TEOS-10: The International thermodynamic equation of seawater – 2010: calculation and use of thermodynamic properties.," *Manuals and Guides*, vol. 56, 2015. Publisher: UNESCO.

[17] J. Jonsson, K. Smedfors, L. Nyholm, and G. Thornell, "Towards Chip-Based Salinity Measurements for Small Submersibles and Biologgers," *International Journal of Oceanography*, vol. 2013, no. 1, p. 529674, 2013. _eprint: https://onlinelibrary.wiley.com/doi/pdf/10.1155/2013/529674.

[18] S.-B. Scientific, "How accurate is salinity measured by my CTD? What factors impact accuracy?."

[19] D. Roemmich, G. C. Johnson, S. Riser, R. Davis, J. Gilson, W. B. Owens, S. L. Garzoli, C. Schmid, and M. Ignaszewski, "The Argo Program," *Oceanography*, vol. 22, no. 2, pp. 34–43, 2009. Publisher: Oceanography Society.

[20] R. J. Uncles, "Estuarine Physical Processes Research: Some Recent Studies and Progress," *Estuarine, Coastal and Shelf Science*, vol. 55, pp. 829–856, Dec. 2002.

[21] C. Canales, "Electrochemical Impedance Spectroscopy and Its Applications," pp. 1–21, Dec. 2021.

[22] E. Barsoukov and J. R. Macdonald, eds., *Impedance Spectroscopy: Theory, Experiment, and Applications*. Wiley, 1 ed., Apr. 2005.

[23] M. Orazem and B. Tribollet, *Electrochemical Impedance Spectroscopy. Wiley-Interscience, New York.* Feb. 2008.

[24] V. Bongiorno, S. Gibbon, E. Michailidou, and M. Curioni, "Exploring the use of machine learning for interpreting electrochemical impedance spectroscopy data: evaluation of the training dataset size," *Corrosion Science*, vol. 198, p. 110119, Apr. 2022.

[25] Y. Xu, C. Li, Y. Jiang, M. Guo, Y. Yang, Y. Yang, and H. Yu, "Electrochemical Impedance Spectroscopic Detection of E.coli with Machine Learning," *Journal of The Electrochemical Society*, vol. 167, p. 047508, Feb. 2020. Publisher: IOP Publishing.

[26] "What Is a Neural Network? | IBM," Oct. 2021.

[27] Christopher M. Bishop, *Pattern Recognition and Machine Learning*. Springer, 2006.

[28] K.-L. Hsueh, "A Study of Artificial Neural Networks for Electrochemical Data Analysis," *Journal of the Chinese Chemical Society*, vol. 57, Aug. 2010.

[29] "What Is Random Forest? | IBM," Oct. 2021.

[30] H. Salman, A. Kalakech, and A. Steiti, "Random Forest Algorithm Overview," *Babylonian Journal of Machine Learning*, vol. 2024, pp. 69–79, June 2024.

[31] "A Table of Electrical Conductivity and Resistivity of Common Materials." Section: ThoughtCo.

[32] R. H. Tyler, T. P. Boyer, T. Minami, M. M. Zweng, and J. R. Reagan, "Electrical conductivity of the global ocean," *Earth, Planets and Space*, vol. 69, p. 156, Nov. 2017.

[33] H. Zhang and X. Xue, "The research progress on corrosion and protection of silver layer," *SN Applied Sciences*, vol. 1, p. 464, Apr. 2019.

[34] D. Sarode, U. Saharkar, H. Ahire, M. Darade, S. Chougule, S. Dalvi, and A. Kurhade, "Corrosion-Resistant Materials for Ocean Structures: Innovations, Mechanisms, and Applications," *Sustainable Marine Structures*, July 2025.

[35] W. A. Roshen, "Fringing Field Formulas and Winding Loss Due to an Air Gap," *IEEE Transactions on Magnetics*, vol. 43, pp. 3387–3394, Aug. 2007.

[36] C. Clark, *The Design of Salinity Sensor for Antarctic Research*. B.Sc Thesis, University of Cape Town, Cape Town, 2024.

[37] S. Jiang and S. Georgakopoulos, "Electromagnetic Wave Propagation into Fresh Water," *Journal of Electromagnetic Analysis and Applications*, vol. 3, pp. 261–266, July 2011. Publisher: Scientific Research Publishing.

[38] J. Wang, B. Jiang, Y. Ou, X. Wang, X. Wei, and H. Dai, "A deep learning-based parameter identification approach of electrochemical impedance spectrum equivalent model for lithium-ion batteries," in *2024 IEEE Transportation Electrification Conference and Expo, Asia-Pacific (ITEC Asia-Pacific)*, pp. 978–983, Oct. 2024.

[39] D. Doonyapisut, P.-K. Kannan, B. Kim, J. K. Kim, E. Lee, and C.-H. Chung, "Analysis of Electrochemical Impedance Data: Use of Deep Neural Networks," *Advanced Intelligent Systems*, vol. 5, no. 8, p. 2300085, 2023. _eprint: https://advanced.onlinelibrary.wiley.com/doi/pdf/10.1002/aisy.202300085.

[40] W. Chen, B. Yan, A. Xu, X. Mu, X. Zhou, M. Jiang, C. Wang, R. Li, J. Huang, and J. Dong, "An intelligent matching method for the equivalent circuit of electrochemical impedance spectroscopy based on Random Forest," *Journal of Materials Science & Technology*, vol. 209, pp. 300–310, Feb. 2025.

[41] A. Alwosheel, S. van Cranenburgh, and C. G. Chorus, "Is your dataset big enough? Sample size requirements when using artificial neural networks for discrete choice analysis," *Journal of Choice Modelling*, vol. 28, pp. 167–182, Sept. 2018.

Appendix A

Additional Files and Schematics

Add any information here that you would like to have in your project but is not necessary in the main text. Remember to refer to it in the main text. Separate your appendices based on what they are for example. Equation derivations in Appendix A and code in Appendix B etc.

IMPORTANT: Appendix A (see the table below) should provide a summary of how you have met the GAs associated with the course, and where in the report the evidence can be found.

If you have used AI in writing your report, you need to provide details in one of the appendices of how you used it.

If appropriate, in a subsequent appendix, provide a link to any GitHub repository where the code and additional materials for your project can be found.

GA	Requirement	Justification and section in the report
1	Problem-solving	Description here
4	Investigations, experiments and data analysis	Description here
5	Use of engineering tools	Description here
6	Professional and technical communication (Long report)	Description here
8	Individual work	Description here
9	Independent learning ability	Description here

Appendix B

Addenda

B.1   Ethics Forms

Appendix C

GitHub Repository

Click here to access the GitHub repository.

GitHub Structure